Astronomical & Astrophysical Transactions

The Journal of the Eurasian Astronomical Society

J = 1-0 HCN towards bright far-infrared sources: Observational data and results of modelling

L. Pirogov [a]; A. Lapinov [a]; I. Zinchenko [a]; V. Shul'ga [b]
[a] Institute of Applied Physics of the Russian Academy of Sciences, Nizhny Novgorod, Russia
[b] Radio Asronomical Institute of the Ukrainian Academy of Sciences, Khar'kov, Ukraina

PLEASE SCROLL DOWN FOR ARTICLE

$J = 1$–0 HCN TOWARDS BRIGHT FAR-INFRARED SOURCES: OBSERVATIONAL DATA AND RESULTS OF MODELLING

L. PIROGOV[1], A. LAPINOV[1], I. ZINCHENKO[1], and V. SHUL'GA[2]

[1] *Institute of Applied Physics of the Russian Academy of Sciences, Uljanov st. 46, 603600 Nizhny Novgorod, Russia*
[2] *Radio Asronomical Institute of the Ukrainian Academy of Sciences, Chervonopraporna st. 4, Khar'kov 310002, Ukraina*

Results of $J = 1$–0 HCN observations of 17 bright far-infrared sources are reported and analyzed. These objects have been observed earlier in the $J = 1$–0 CO line. HCN column densities and abundances have been calculated for two objects. The correlations between peak HCN and CO temperatures, HCN linewidths and FIR luminosities, HCN linewidths and masses of the objects are revealed. HCN and CO intergrated intensities do not correlate with FIR luminosities. The R_{12} intensity ratios of the $J = 1$–0 HCN hyperfine structure for several objects are less than expected for optically thin case while the HCN linewidths are much greater than thermal ones for possible kinetic temperatures of the dense gas. This fact cannot be explained in the framework of the model with constant turbulent velocity over the cloud. The possible cloud model for these objects should implement inhomogeneous turbulent velocity and density structure.

KEY WORDS   Interstellar clouds, molecules: HCN, infrared sources, modelling

1 INTRODUCTION

Investigations of dense gas in star-forming regions can improve our knowledge about the relationship between parameters of young stellar objects and the parent cloud. Observations of large samples of objects can give an opportunity to use methods of statistical analysis which are very fruitful in revealing general properties of the sample under the study. Recently, a sample of 40 bright FIR sources ($F_{100} > 500$ Jy) located in the outer Galaxy was investigated by Snell *et al.* [1, 2] in the $J = 1$–0 CO line. They searched for energetic molecular outflows near young stellar objects. These objects plus 11 sources included in Lada's review [3] form the full sample of bright FIR sources ($F_{100} > 500$ Jy) from the IRAS Point Source Catalog [4] with right ascension between R.A. 0^h and 12^h and declination greater than $0°$. Lately,

nearly half of these sources were investigated by Carpenter *et al.* [5, 6] in the $J = 1$-0 CO, $J = 1$-0 ^{13}CO and $J = 2$-1 CS lines and 6 cm radio continuum. The clouds observed in the CO line [5] were found to be in virial equilibrium; a strong correlation between the cloud masses and CO-luminosities was found [5].

In this paper we present results of $J = 1$-0 HCN observations toward 17 galactic star-forming regions which have been observed earlier in the CO line [1, 2]. The $J = 1$-0 HCN observations were performed in October 1994 at the RT-22 radiotelescope of the Crimean Astrophysical Observatory. The main goal of our investigations, besides searching for dense gas emission in molecular clouds associated with bright FIR sources, was to study physical properties of the dense gas by comparing the parameters of different molecular lines with each other and with parameters of the FIR sources. The $J = 1$-0 HCN and HCO$^+$ surveys performed a few years ago [7, 8, 9] helped to reveal some correlations between molecular line parameters in the clouds associated with Sharpless H II regions. The same analysis for a sample of bright FIR sources in the outer Galaxy, for which the CO, data exist could give a valuable information on the physical properties of the objects. The RT-22 beam width (40″) at 88.6 GHz (the $J = 1$-0 HCN line frequency) is close to the spatial resolution of the $J = 1$-0 CO observations [1, 2] which is useful for comparing the data. Because the distances to the objects are known, we have been able to derive the FIR luminosities and masses of the objects and to use these quantities in our analysis. The low-noise 3 mm maser receiver used in our observations [10] has given opportunity to detect all three $J = 1$-0 HCN hyperfine components with high signal-to-noise ratio in most objects observed. We have compared the observed line intensities with the results of computer simulations.

2 OBSERVATIONS

The $J = 1$-0 HCN observations (at a frequency 88631.8 MHz) were performed in October 1994 with the 22-m radiotelescope of the Crimean Astrophysical Observatory. The radiometer was equipped with a maser amplifier at the front end [10]. The receiver single sideband noise temperature was ~ 60 K, the input frequency bandwidth was 40 MHz. Spectral resolution was 100 KHz (~ 0.33 km/s). The total bandwidth of the spectrum analyzer was 12 MHz. The telescope HPBW (40″) was estimated from observations of planets and strong continuum point-like sources. The pointing accuracy was $\sim 20″$. The main beam efficiency (~ 0.3) was evaluated from the comparison of our $J = 1$-0 HCN observations of Orion KL with the results obtained with the 20-m radiotelescope in Onsala [11]. We express the line intensities in units of the main beam temperature T_{MB}. Methods of observation and calibration as well as data reduction were the same as those described earlier [7, 9].

The list of 17 sources observed in the $J = 1$-0 HCN line is given in Table 1. Here we give the coordinates and the distances to the objects. The latter values, which correspond to the distances to the H II regions and OB associations that lie near the FIR sources, were taken from [1, 2].

Table 1.   The source list: coordinates and distances to the objects

Name	α(1950) (^{h}) (^{m}) (^{s})	δ(1950) (°) (') ('')	D (kpc)	Reference
00338+6312	00 33 53.3	63 12 32	1.6	[2]
02230+6202	02 23 02.3	62 02 24	2.2	[1]
02244+6117	02 24 27.2	61 17 47	2.2	[2]
02575+6017	02 57 35.6	60 17 22	2.2	[1]
03064+5638	03 06 26.9	56 38 56	4.1	[1]
03211+5446	03 21 11.8	54 46 51	3.1	[1]
04073+5102	04 07 18.5	51 02 30	12.1	[2]
04324+5106	04 32 28.7	51 06 39	6.0	[1]
05100+3723	05 10 01.7	37 23 35	2.6	[1]
05197+3355	05 19 46.4	33 55 39	3.2	[2]
05274+3345	05 27 27.6	33 45 37	1.8	[1]
05345+3157	05 34 32.6	31 57 40	1.8	[1]
05355+3039	05 35 34.0	30 39 48	1.8	[1]
05358+3543	05 35 48.8	35 43 41	1.8	[2]
05375+3540	05 37 32.1	35 40 45	1.8	[2]
05377+3548	05 37 46.7	35 48 25	1.8	[2]
06013+3030	06 01 21.2	30 30 53	4.7	[2]

3   RESULTS AND DATA ANALYSIS

3.1   Observational Results and Comments on Individual Objects

We observed 17 IRAS sources which were arbitraryly selected from the sample of bright FIR sources [1, 2]. Each source was observed at one point corresponding to the IRAS point source position which coincides with the position of the CO peak emission in most cases. HCN emission was detected in 14 cases.

Spectra for 8 sources are shown in Figure 1. The three hyperfine components are clearly distinguishable and do not overlap in most cases.

A few sources demonstrate a complex structure. An example is 00338+6312 where two components (at ~ -19 km/s and ~ -16 km/s, respectively) are most probably the result of deep self-absorption. The high-velocity wing component is also seen in the HCN spectrum in this source. We fitted the spectrum by 3-component gaussian. Note, that we considered parameters of this fit only as convenient numerical representation of the line profile with self-absorption and did not use them in the following analysis.

Asymmetric lines were detected also in 05274+3345 where we probably see emission of two fragments lying on the line of sight. The hyperfine components of these fragments overlap, which makes it difficult to interpret the spectrum. Therefore we excluded the data for this source from the following analysis.

An outflow is probably seen toward 02575+6017 but the outflow velocity is not very high. A red emission wing probably exists also in 05358+3543. The high-velocity intensity in these sources is close to the detection limit; thus, we do not try to determine parameters of the outflows.
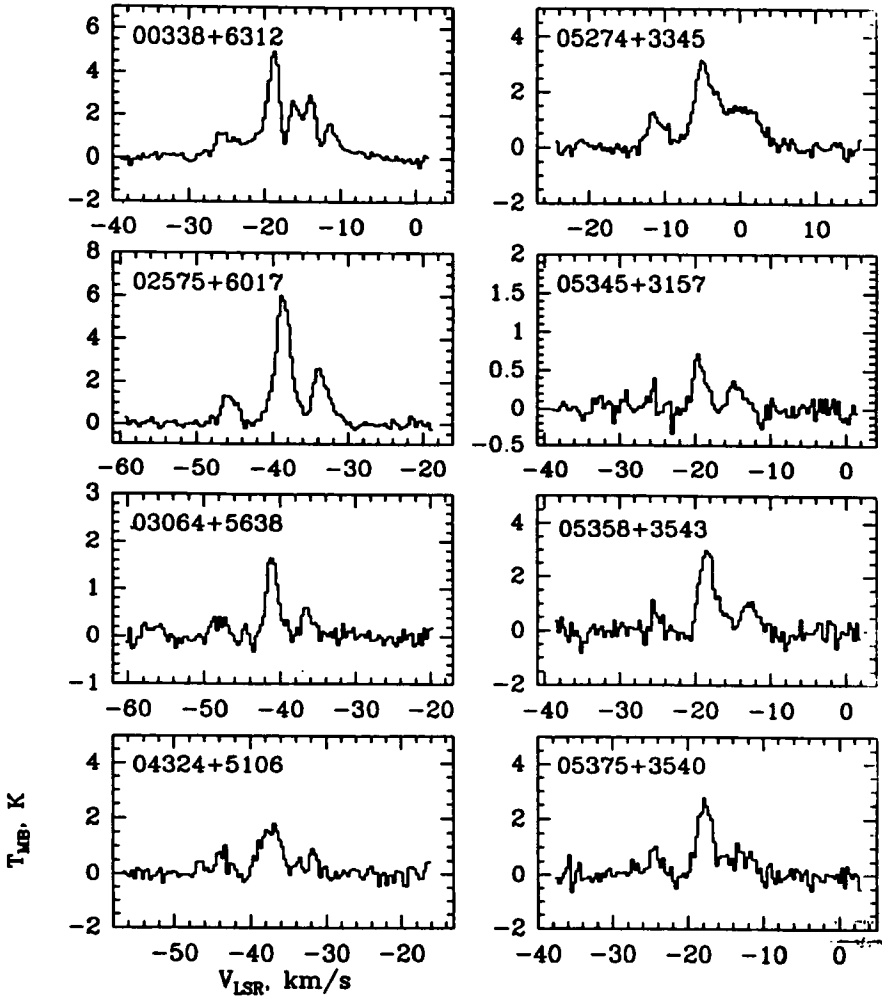
Figure 1   The $J = 1$–0 HCN spectra toward 8 objects from the observed sample of bright FIR sources. Three components of the $J = 1$–0 HCN hyperfine structure ($F = 0$–1, $F = 2$–1 and $F = 1$–1) are clearly visible on the spectra shown.

The spectra obtained were fitted with one, two or three gaussian triplets with fixed separations between the hyperfine components. Table 2 presents the results of gaussian fits to the HCN spectra. For those sources where the HCN emission was not detected, the upper limits (3σ values) on the main beam temperature are given. The CO data from Snell *et al.* [1, 2] are also included in Table 2.

The results of fitting by two HCN triplets are also presented for three sources. For 00338+6312 two of three HCN triplet parameters with exception of high-velocity component are given in Table 2. HCN and CO LSR velocities are equal to each other with allowance for uncertainties of their determination.

Table 2.   The $J = 1$–0 HCN and CO line parameters for bright FIR sources

Name	$J = 1$–0 HCN					$J = 1$–0 CO			Reference
	T_{MB} (K)	V_{lsr} (km/s)	ΔV (km/s)	R_{12}	R_{02}	T_R^* (K)	V_{lsr} (km/s)	ΔV (km/s)	
00338+6312	4.1(1)	−18.91(2)	1.40(3)	.54(4)	.16(4)	13.2	−18.4	5.5	[2]
(RNO 1)	1.7(2)	−16.07(4)	1.38(8)	.7(1)	.0(1)				
02230+6202	< .6					9.1	−43.0	3.8	[1]
(W3 N)									
02244+6117	0.44(6)	−51.0(2)	3.2(2)	.6(1)	.4(1)	15.6	−50.8	5.0	[2]
02575+6017	5.8(1)	−38.60(2)	2.41(2)	.43(2)	.22(2)	23.8	−38.9	5.5	[1]
(IC 1848)									
(S 199)									
03064+5638	1.7(1)	−41.10(4)	1.73(6)	.34(5)	.23(4)	8.6	−39.8	2.4	[1]
03211+5446	< .75					5.0	−31.3	1.9	[1]
04073+5102	0.4(1)	−53.8(1)	1.3(2)	−.7(5)	.6(3)	5.8	−53.2	3.9	[2]
(S 209)	0.6(2)	−48.5(3)	4.3(5)	.4(2)	.2(1)				
04324+5106	1.7(1)	−37.3(1)	3.0(1)	.30(6)	.35(6)	9.1	−35.6	5.7	[1]
(WB 573)									
05100+3723	0.5(1)	−7.1(2)	3.4(3)	.4(1)	.0(1)	11.7	−6.4	4.0	[1]
(S 228)									
05197+3355	0.4(1)	−4.9(2)	1.9(2)	.8(3)	.7(3)	20.4	−4.0	2.7	[2]
(S 230)									
05274+3345	2.0(5)	−5.4(1)	1.9(2)	.3(2)	.1(1)	12.6	−4.1	5.5	[1]
	1.9(2)	−3.7(4)	3.5(3)	.7(1)	.5(1)				
05345+3157	0.64(5)	−19.4(8)	2.1(1)	.54(9)	.20(6)	9.9	−17.7	5.2	[1]
(WB 671)									
05355+3039	0.67(7)	−16.6(1)	1.7(1)	.6(1)	.3(1)	5.7	−15.8	4.1	[1]
(WB 678)									
05358+3543	3.0(1)	−18.3(1)	2.5(1)	.35(5)	.17(5)	17.0	−18.2	5.3	[2]
(S 233)									
05375+3540	2.5(2)	−17.7(1)	2.6(1)	.37(5)	.30(5)	20.9	−17.2	4.1	[2]
(S 235B)									
05377+3548	3.6(3)	−20.4(1)	2.2(1)	.6(1)	.0(1)	23.9	−20.0	4.5	[2]
(S 235)									
06013+3030	< .85					2.1	2.7	3.3	[2]

3.2   Mass determination

Using extended FIR emission maps (ISSA) we determined for each source of our sample integrated FIR fluxes at 4 wavelengths ($12\mu m$, $25\mu m$, $60\mu m$ and $100\mu m$) within $5'$ around the *IRAS* point source position. These areas likely include most of the dense molecular gas associated with the FIR source. Using a two-component FIR source model [12], we calculated dust temperatures (cold and hot components) and FIR luminosities for these sources. We calculated then gas masses for the objects under the study using the following relation [13]:

$$M = 4 \cdot D^2 \cdot \frac{F_{100}}{B_{100}(T_D)}, \tag{1}$$

Table 3. FIR luminosities, dust temperatures (cold component) and masses the 5' around bright FIR sources. The dust emissivity index is assumed to be equal to 1. Masses determined from CS and CO observations [6] are also given for 9 objects

Name	$L_{FIR}(r < 5')$ ($L_{\odot}$)	T_D (K)	M (fromFIR) ($M_{\odot}$)	M (fromCS) ($M_{\odot}$)	M (fromCO) ($M_{\odot}$)
00338+6312	2.4×10^3	34	60	140	1300
02230+6202	7.0×10^4	49	220		
02244+6117	3.1×10^4	36	560		
02575+6017	1.2×10^4	39	110	200	2800
03064+5638	2.8×10^4	37	420	8	150
03211+5446	2.1×10^4	38	270		
04073+5102	1.6×10^6	45	7930		
04324+5106	5.3×10^4	39	560	1000	5400
05100+3723	1.1×10^4	41	80	12	380
05197+3355	1.3×10^4	38	170	13	750
05274+3345	4.0×10^3	35	90	150	1800
05345+3157	3.1×10^3	37	40		
05355+3039	4.5×10^3	38	60		
05358+3543	6.3×10^3	36	110		
05375+3540	2.0×10^4	40	190	206	3600
05377+3548	2.3×10^4	38	290	196	3800
06013+3030	4.0×10^4	40	390		

where D is the distance to the object, F_{100} is the flux at 100μm, $B_{100}(T_D)$ is the Plank function for dust temperature T_D (cold component) at $\lambda = 100\mu$m. The numerical coefficient represents the mass opacity at $\lambda = 100\mu$m when the dust emissivity index is equal to unity [13]. If the dust emissivity index is equal to 2, the calculated masses decrease by 10–15%.

FIR luminosities of the IRAS sources, dust temperatures and masses are given in the Table 3. For 9 objects in our sample the masses have been determined by Carpenter *et al.* [6] from the $J = 2 - 1$ CS line. Although there is no correlation between these masses and our FIR-based masses, with few exceptions they have the same order of magnitude and differ by an order of magnitude from the corresponding masses traced by the CO line. Masses determined from CS and CO observations [6] are also given in Table 3.

3.3 H_2 Column Densities and HCN Abundances

The relative intensities of the satellite components of the $J = 1$–0 HCN hyperfine structure ($R_{12} = T_{\rm MB}(F = 1$-$1)/T_{\rm MB}(F = 2$-$1)$ and $R_{02} = T_{\rm MB}(F = 0$-$1)/T_{\rm MB}(F = 2$-$1))$ for two objects (05345+3157 and 05355+3039) are close to the optically thin values ($R_{12} = 0.6$, $R_{02} = 0.2$). Under the LTE assumption and adopting an excitation temperature equal to 10 K, the HCN column densities, $N_{\rm HCN}$, for these objects have been calculated using formulae (2) from [22]. They are summarized in Table 4.

Table 4.   HCN and H_2 column densities and HCN abundances for two
objects with optically thin HCN emission

Name	$N_{HCN} \times 10^{-12}$ $(cm^{-2}$	$N_{H_2} \times 10^{-22}$ (cm^{-2})	$X_{HCN} \times 10^9$
05345+3157	3.8	1.0	0.4
05355+3039	3.5	0.5	0.7

Then we calculated then the molecular hydrogen column densities for these objects using the empirical relation between CO integrated intensity, $I(CO)$, and molecular hydrogen column density (N_{H_2}):

$$N_{H_2} = W \cdot I(CO). \qquad (2)$$

The coefficient W was assumed to be equal to 2×10^{20} cm^{-2} (K km/s)$^{-1}$ (see a discussion of a possible range of W-values in [14]). The hydrogen column densities are also summarised in the Table 4. Both hydrogen and HCN column densities correspond to regions with nearly the same ($\sim 40''$) diameter. The HCN abundances for these two sources ($X_{HCN} = N_{HCN}/N_{H_2}$) are given in the column 4 of the Table 4.

These values are ~ 10 times lower than the "standard" X_{HCN} values obtained in OMC-1 (5×10^{-9}) and Sgr B2 (3×10^{-9}) using other methods [15]. The discrepancy in general could arise both from the uncertainty of the W-value and HCN abundance variotions in molecular clouds.

3.4   Comparion of the HCN, CO and FIR Data

We notice first that, because we did not observe a full sample of the sources, the following analysis is not free from bias and incompleteness effects.

Figure 2 shows a plot of the HCN main beam temperature ($F = 2$–1 component) versus CO brightness temperature. There is some tendency of increase in the HCN temperature with the CO one (correlation coefficient is ~ 0.6). However, the scatter is large. This fact can be connected both with density variations in the objects as well as with the difference between $T_R^*(CO)$ and gas kinetic temperature in the dense regions of the clouds emitting in the $J = 1$–0 HCN line.

Figure 3 displays the HCN linewidth (FWHM) versus the CO one. The HCN linewidths are seen to be smaller than the corresponding CO widths by a factor of ~ 2. For the objects observed by Carpenter *et al.* [5] (18 objects) we found some correlation between ΔV and CO emission region size (correlation coefficient is equal to 0.6). If that correlation reflects a real dependence between the molecular linewidth and cloud size then the smaller HCN linewidths could indicate the smaller emission region sizes for HCN in comparison with the CO ones.

Neither the CO nor HCN integrated intensities show any correlation with the FIR luminosities. A slight correlation after excluding one "bad" point probably exists between the CO luminosities for the objects observed by Carpenter *et al.* [5] and the FIR luminosities.
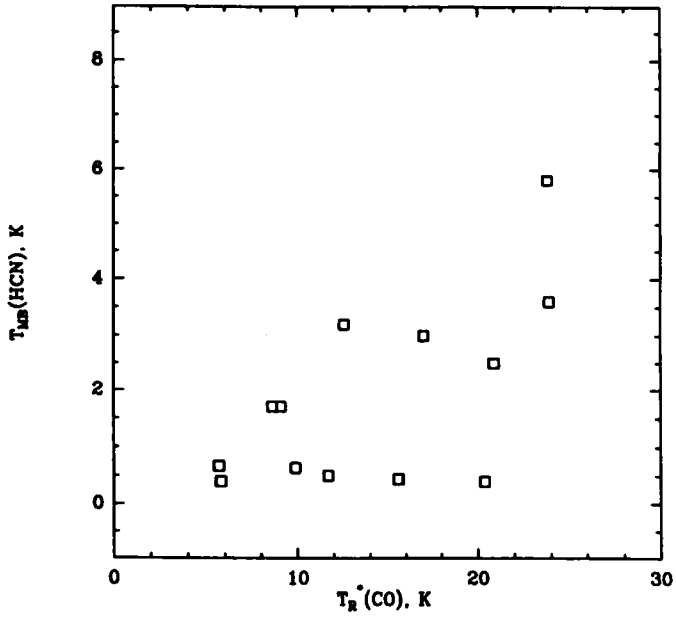
Figure 2   The HCN main beam temperature ($F = 2$–1 component) versus $T_R^*(CO)$ temperature. The correlation coefficient between these quantities is ~ 0.6.

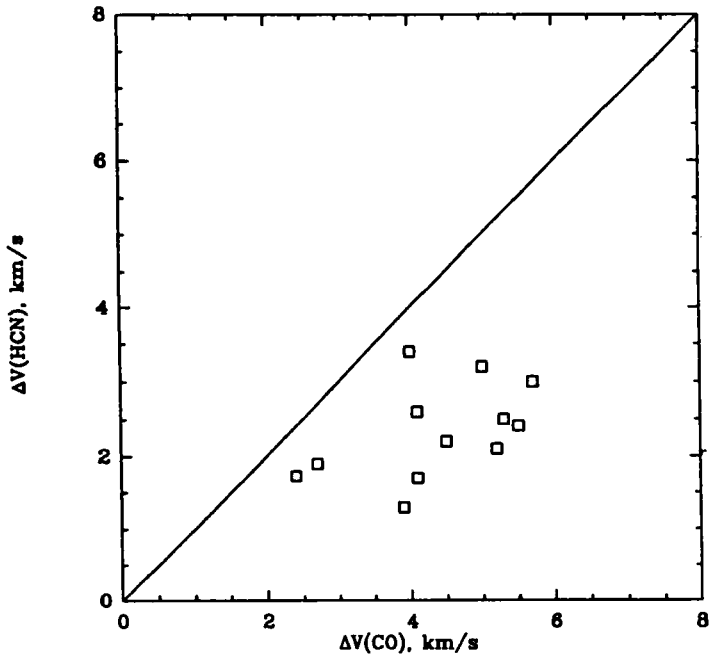**Figure 3**   The HCN linewidths (FWHM) versus CO ones. The HCN linewidths are systematically lower than CO linewidths. The line $\Delta V(HCN) = \Delta V(CO)$ is also shown on the figure.
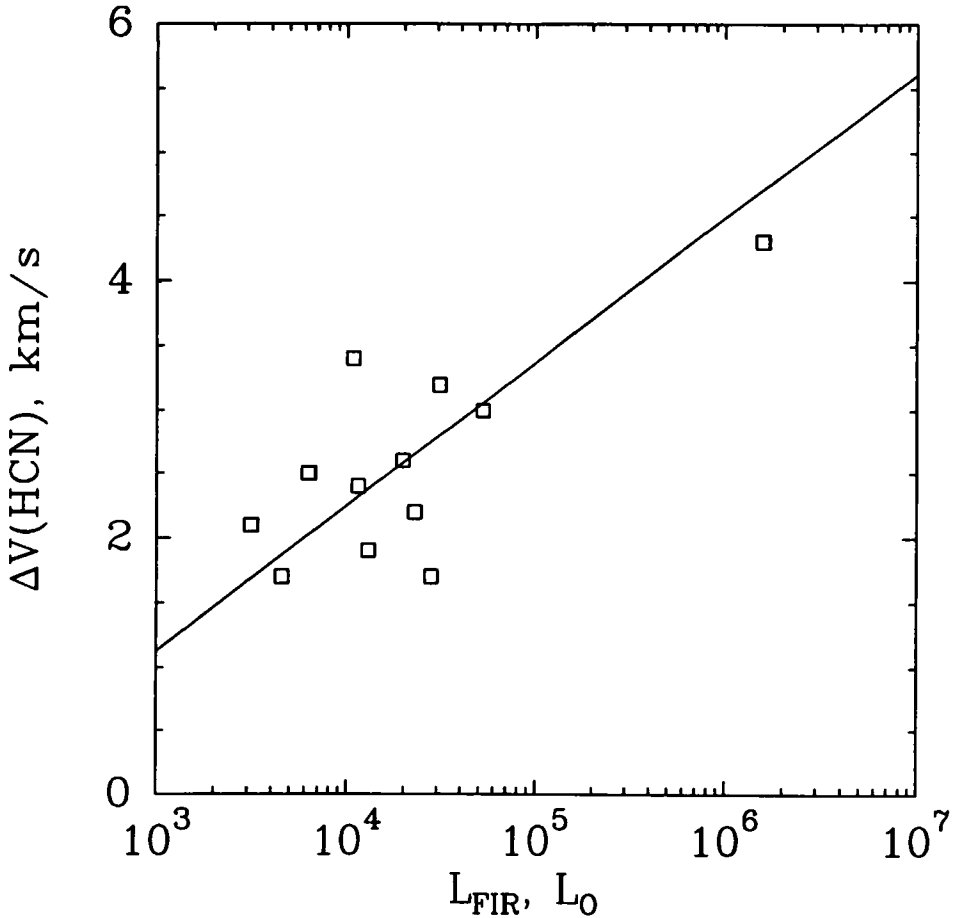
Figure 4 The HCN linewidth versus FIR luminosity derived for regions of 5' radius with an IR point source at the center. The least squares fit $\Delta V(km/s) = -2.3 + 1.1\log(L_{FIR})$ is also shown. The correlation coefficient is 0.7.

In Figure 4 we plot the HCN linewidth versus logarithm of the FIR luminosity for those objects where we detected HCN (with the exception of 05274+3345 and 00338+6312). The least squares fit (correlation coefficient = 0.7) is also shown in the figure. This dependence probably indicates an influence of the FIR source on the HCN line broadening. For comparison we notice that the CO line widths, ΔV_{CO} do not correlate with L_{FIR}.

In Figure 5 we show the HCN linewidth versus the mass of a cloud (as a given in Table 3) with both quantities given in the logarithmic scale. The least squares fit (correlation coefficient = 0.6 is also shown. The slope of this regression line (0.2) is equal to the one found by Larson [16] but our line is shifted towards higher ΔV values. The explanations of such a correlation is usually based on the assumption of virial equilibrium of the clouds.
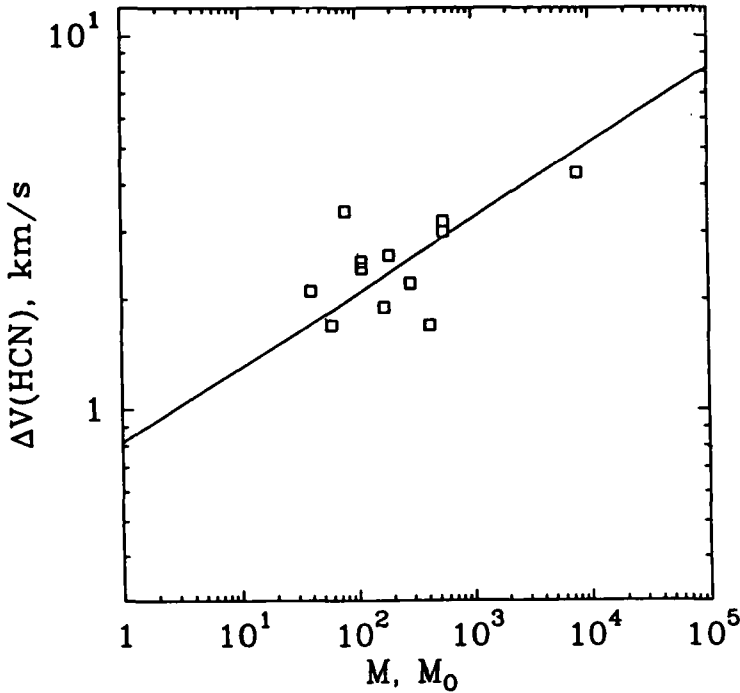
Figure 5 The HCN linewidth versus mass. The least squares fit $\Delta V(\text{km/s}) = 0.8 \times M^{0.2}$ is also shown. The correlation coefficient is 0.6.

4 RESULTS OF MODELLING

4.1 The R_{12} Ratios and the Microturbulent Model with Constant Turbulent Velocity

In Figure 6 the R_{12} and R_{02} HCN hyperfine intensity ratios are shown versus the CO temperature for those clouds where the satellite components of the $J = 1$–0 HCN were detected with high signal-to-noise ratio. The optically thin values for the R_{12} and R_{02} ratios (0.6 and 0.2, respectively) are shown by horizontal lines. One can see that in several sources the R_{12} ratio is smaller than the optically thin value.

Usually in the clouds with kinetic temperature of about 10 K (dark clouds) the observed R_{12} ratio is equal to or exceeds the optically thin value. In warm clouds where kinetic temperature is about 30 K or higher the observed R_{12} ratio is usually less than 0.6. These facts can be explained by the overlap of the hyperfine components in the $J = 2$–1 HCN transition [17]. In spite of the fact that theory [17] predicts the corresponding decrease of the R_{02} ratio with respect to the optically thin value (0.2) this effect is not evident for the observed objects. Therefore in the following discussion only the observed and model R_{12} ratios will be compared.
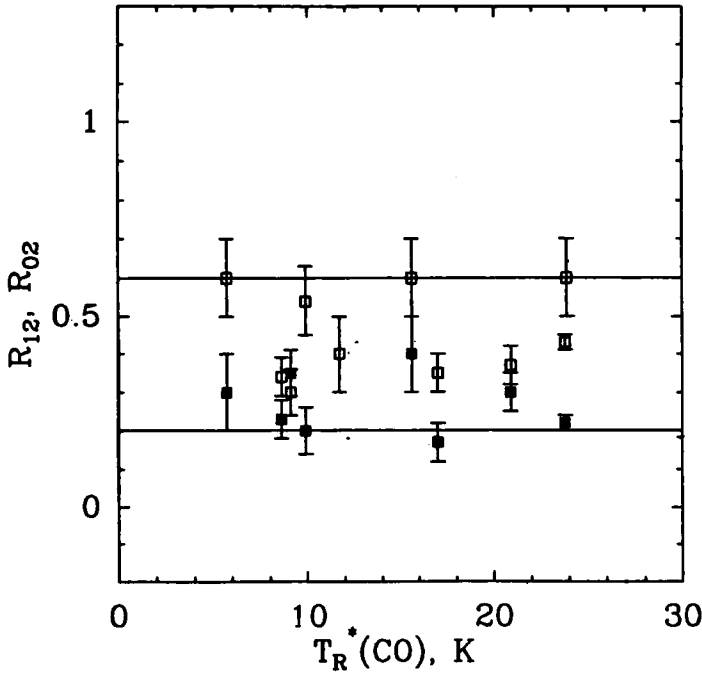
Figure 6 R_{12} (open squares) and R_{02} (filled squares) HCN hyperfine intensity ratios versus the $T_R^*(CO)$ temperature. Horizontal lines are drawn at 0.6 and 0.2 levels, the values of R_{12} and R_{02} in the optically thin case, respectively.

In Figure 7 the R_{12} ratio is shown versus the HCN linewidth. In spite of the fact that there is no strong correlation between these quantaties, there is some trend for decrease in R_{12} with increasing ΔV_{HCN}.

However, the homogeneous isothermal microturbulent cloud model, where local profile linewidths are equal to the observed linewidths, fails to fit the observed $J = 1$-0 HCN intensities in most objects where the R_{12} ratio is lower than the optically thin value (0.6). This can be explained by the fact that the effect of the hyperfine component overlaps in the $J = 2$-1 HCN transition which causes R_{12} to decrease below the optically thin value [17] is not effective when the local linewidths become much greater than the thermal ones.

We performed simulations with a microturbulent model for the HCN excitation in a homogeneous isothermal cloud model where the local HCN lines have the microturbulent broadening in addition to the thermal one. For the cloud model with $T_{KIN} = 10$ K we used the Monteiro–Stutzki [18] HCN–H_2 collisional rates which seem to be more appropriate for the lower temperatures while for the cloud model with $T_{KIN} = 30$ K we used the Varshalovich–Khersonsky [19] HCN–He collisional rates. The minimum values of the R_{12} ratio obtained in models with different values of kinetic temperatures, densities and turbulent velocities are given in Table 5.

Table 5.   The minimum values of R_{12} obtained in microturbulent cloud models

		$V_{TURB} = 1.0 \, km/s$	$V_{TURB} = 1.3 \, km/s$
$T_{KIN} = 10$ K	$n = 10^4$ cm^{-3}	0.51[a]	0.58[a]
	$n = 10^5$ cm^{-3}	0.59[a]	0.60[a]
	$n = 10^6$ cm^{-3}	0.60[a]	0.60[a]
$T_{KIN} = 30$ K	$n = 10^4$ cm^{-3}	0.43[b]	0.54[b]
	$n = 10^5$ cm^{-3}	0.41[b]	0.55[b]
	$n = 10^6$ cm^{-3}	0.47[b]	0.55[b]

Note.   [a] The Monteiro–Stutzki HCN–H_2 collisional rates [18].
[b] The Varshalovich–Khersonsky HCN–He collisional rates [19].

The value of $V_{TURB} = 1.0$ km/s corresponds to the smallest HCN linewidth (1.6 km/s) in our sample. One can see that for $V_{TURB} = 1.0$ km/s and $T_{KIN} = 10$ K, the minimum value of R_{12} is equal to 0.51 only for the density of 10^4 cm^{-3} while for $T_{KIN} = 30$ K and the same turbulent velocity for all a densities considered the minimum R_{12} values are ~ 0.4–0.5. However, taking $V_{TURB} = 1.3$ km/s which corresponds to $\Delta V_{FWHM} = 2.2$ km/s, the R_{12} minimum values differ only slightly from the optically thin value (0.6) in only case. Further increase in V_{TURB} causes the minimum values to be exactly equal to 0.6.

In Figure 7 we have also ploted the minimum values of R_{12} obtained in one of the microturbulent models described ($T_{KIN} = 30$ K, $n = 10^5$ cm^{-3}) versus ΔV(HCN). This quantity rises quickly from about 0.3 (ΔV(HCN) = 1.4 km/s) to 0.6 (ΔV(HCN) ~ 2 km/s) and then remains constant. It is clear from this figure that the model fails to fit most of the observed objects where R_{12} ratios are less than 0.6 but ΔV(HCN) ~ 2 km/s or higher.

4.2   Possible Models of Dense Molecular Cloud Cores and Indications of Inhomogenous Structure

An alternative approach to fit the model HCN spectra to the observed ones could be with inhomogeneous distribution of turbulent velocities over the cloud. In such a model the resulting peak intensities of the HCN components from which one derives the R_{12} and R_{02} ratios should arise in those parts of the clouds where the turbulent velocities are small enough to produce the observed R_{12} anomalies. These parts of the clouds in turn should be the densest ones to produce smooth line profiles without self-reversals. The line wing emission should arise in the parts of the clouds with smaller densities but with higher turbulent velocities to produce the observed HCN linewidths.

It is known that in the models with systematic motions the R_{12} and R_{02} ratios can vary due to the fact that, because of Doppler shift, even HCN hyperfine components far apart can overlap when originating in different parts of the cloud [20]. For particular cloud geometry with systematic velocity field the R_{12} ratio can decrease below the value of 0.6.
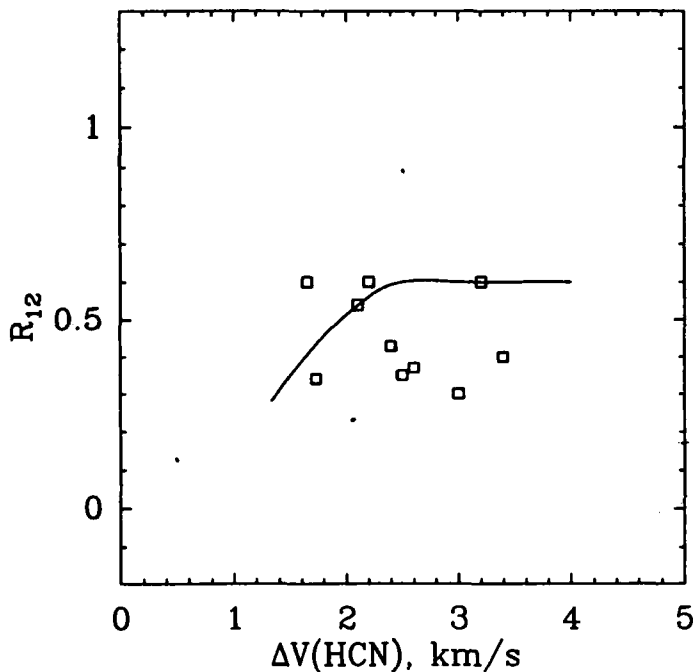
Figure 7 HCN hyperfine intensity ratio R_{12} versus the HCN linewidth (FWHM). The curve correspond to the minimum R_{12} values found in the microturbulent cloud model with constant parameters over the cloud.

To examine the effect of the distant overlaps to the R_{12} and R_{02} ratio variations we have considered the "core+envelope" spherical model similar to the one used in [22] for HCO$^+$ and H^{13}CO$^+$ modelling. The core is assumed to be much denser than the envelope which has in addition a constant velocity of expansion. It was found that the effect of the distant overlaps can cause the R_{12} and R_{02} ratios to vary only if the overlapping components in the $J = 2\text{-}1$ HCN transition are not involved into close overlaps due to local broadening of the line profiles. Therefore, this effect can take place only in regions with very narrow local linewidths and, taken alone, it cannot account for observed ratio anomalies discussed here.

Another possible approach which could reconcile the model molecular spectra with the observed ones could be a clumpy model of the cloud. The simplified version of such a model [21] was treated in [22] where good fits were obtained to the observed HCO$^+$ and H^{13}CO$^+$ spectra in the S140 molecular cloud. In this model the cloud was assumed to contain a large number of dense clumps moving chaotically with respect to each other. Each clump has dimensions much smaller than the telescope beam and is surrounded by low-density medium. Molecular emission lines from a single clump have only thermal broadening. Molecular emission lines from a single clump have only thermal broadening. The result linewidth of the emission line of such an ensemble of clumps reflects the interclump velocity dispersion.

5 CONCLUSIONS

In this paper we have presented results of $J = 1\text{--}0$ HCN observations toward 17
galactic star-forming regions associated with bright FIR IRAS sources which have
been observed earlier in the CO line [1, 2]. The main goal of this investigation was
to search for dense gas emission in the molecular clouds associated with bright FIR
sources and to study its physical properties by comparing different molecular line
parameters with each other and with parameters of the FIR sources.

For two objects of the sample where the relative intensities of the $J = 1\text{--}0$ HCN
satellite components, R_{12} and R_{02}, are close to the optically thin values (0.6 and
0.2, respectively) the HCN column densities were estimated. Using these values
and the H_2 column density estimates from CO data, the HCN abundances were
calculated to lie in the range $(0.4\text{--}0.7) \times 10^{-9}$.

We have calculated masses of the objects using the relationship between the
mass and the FIR flux at $100\mu m$ [13]. Masses of the objects lie in the range (40–
8000)$M_\odot$. The comparison between the HCN, CO [1, 2] data, FIR luminosities and
derived masses of the objects leads to the following conclusions:

- There is some correlation between the HCN temperature $(J = 1\text{--}0, F = 2\text{--}1)$
  and the CO $J = 1\text{--}0$ peak temperatures. The weakness of the correlation
  between these quantities can be due to density variations in the clouds and
  the possible difference between peak CO and gas kinetic temperatures in the
  dense regions of the clouds emitting in the $J = 1\text{--}0$ HCN line.

- The HCN linewidths are lower than CO ones by a factor of ~ 2.

- The HCN and CO integrated intensities do not show any correlation with
  the FIR luminosity. There is some evidence of the correlation between the
  CO-luminosities obtained in [5] are FIR luminosities. We found a correla-
  tion between the HCN linewidth and FIR luminosity and between the HCN
  linewidth and mass of the clouds. The latter dependence probably reflects the
  fact that the objects are in virial equilibrium.

A comparison of the R_{12} intensity ratios with the HCN linewidths shows that R_{12}
does not increase with ΔV_{HCN} in contradiction to the results of the microturbulent
model with constant turbulent velocity.

A possible model which could reproduce the HCN spectra in the objects where
the R_{12} ratios are less than the optically thin value (0.6) is a model where turbulent
velocity increases with radius of the cloud while the cloud density decreases with
radius. An alternative model could be a clumpy model of the cloud where molecular
emission lines of a single clump have only thermal broadening and the resulting
linewidth reflects the interclump velocity dispersion.

5.1 Acknowledgements

the spectrum analyser, A. Zuban' and especially V. Shanin for writing the new software package for our observing program. We are grateful to the administration of the Radioastronomical Laboratory of the Crimean Astrophysical Observatory for providing the observing time, and to the RT-22 control group for excellent radiotelescope functioning. We thank Prof. K. Mattila for critical reading of the manuscript and many valuable comments and corrections. L. P. is very grateful to the Helsinki University Observatory for the hospitality. The work was supported by the ESO C&EE grant A-02-001 and the Russian Foundation for Basic Reseach, grant 94–02–04861–a.

References

1. Snell, R. N., Huang, Y.- L., Dickman, R. L., Clausen, M. J. (1988) *Astrophys. J.* **325**, 853.
2. Snell, R. N., Dickman, R. L., Huang, Y.-L. (1990) *Astrophys. J.* **352**, 139.
3. Lada, C. J. (1985) *Ann. Rev. Astr. Ap.* **23**, 267.
4. IRAS Point Source Catalog (1985) *Joint IRAS Working Group* (Washington, DC: GPO).
5. Carpenter, J. M., Snell, R. N., Schloerb, F. P. (1990) *Astrophys. J.* **362**, 147.
6. Carpenter, J. M., Snell, R. N., Schloerb, F. P., Skrutskie, M. F. (1993) *Astrophys. J.* **407**, 657.
7. Burov, A. B., Vdovin, V. F., Zinchenko, I. I., Kislyakov, A. G., Krasil'nikov, A. A., Kukina, E. P., Lapinov, A. V., and Pirogov L. E. (1988) *Pis'ma v Astron. Zh.* **14**, 492.
8. Zinchenko, I. I., Lapinov, A. V., and Pirogov, L. E. (1989) *Astron. Zh.* **66**, 1142.
9. Zinchenko, I. I., Krasil'nikov, A. A., Kukina, E. P., Lapinov, A. V., and Pirogov, L. E. (1990) *Astron. Zh.* **67**, 908.
10. Shul'ga, V. M., Zinchenko, I. I., Nesterov, N. S., Myshenko, V. V., Andriyanov, A. F., Isaev, V. F., Knyaz'kov, L. B., Lapinov, A. V., Litvinenko, L. N., Mal'tsev, V. A., Pirogov, L. E., Shanin, V. N., and Shtanyuk, A. M. (1991) *Pis'ma v Astron. Zh.* **17**, 1084.
11. Johansson, L. E. B., Andersson, C., Ellder, J., Friberg, P., Hjalmarson, A., Höglund, B., Irvine, W. M., Olofsson, H., and Rydbeck, G. (1984) *Astron. Astrophys.* **130**, 227.
12. Pirogov, L. E. and Zinchenko, I. I. (1993) *Astron. Zh.* **70**, 959.
13. Hildebrand, R. H. (1983) *Quat. Jour. R. A. S.* **24**, 267.
14. Brand, J., Wouterloot, J. G. A. (1994) *Astron. & Astrophys. Suppl.* **103**, 503.
15. Blake, G. A., Sutton, E. C., Masson, C. R., and Phillips, T. G. (1987) *Astrophys. J.* **315**, 621.
16. Larson, R. B. (1981) *Mon. Not. R. A. S.* **194**, 809.
17. Guilloteau, S. and Baudry, A. (1981) *Astron. & Astrophys.* **97**, 213.
18. Monteiro, T. S. and Stutzki, J. (1986) *Mon. Not. Roy. Astron. Soc.* **221**, 33 p.
19. Varshalovich, D. A. and Khersonsky, V. K. (1977) *Astrophys. Lett.* **18**, 167.
20. Zinchenko, I. and Pirogov, L. (1987) *Astron. Zh.* **64**, 483.
21. Martin, H. M., Sanders, D. B., Hills, R. E. (1984) *Mon. Not. Roy. Astron. Soc.* **208**, 35.
22. Pirogov, L. E., Zinchenko, I. I., Lapinov, A. V., Shul'ga, V. M., Myshenko, V. V. (1995) *Astr. & Astrophys. Suppl.* **109**, 333.